# Impact of graphene oxide and highly reduced graphene oxide on cement based composite

Tanvir S Qureshi[a*] and Daman K Panesar[a]

[a] Department of Civil Engineering, University of Toronto, Toronto, Ontario M5S 1A4, Canada

*Corresponding author: e-mail: d.panesar@utoronto.ca; Tel.: +1-416-946-5712

**Abstract:**

This study examines and compares the performance of two specific forms of graphene nanomaterials in the cement based composite, namely graphene oxide (GO) and reduced graphene oxide (rGO). A typical forms of GO with the average C:O ratio of 54:46 and a rGO with the average C:O ratio of 82:18 were used in the cement based paste composites. rGO was treated with superplasticizer to improve its dispersibility in water. Both GO and rGO were used as 0.02, 0.04, 0.06 wt% of cement. The effect of GO and rGO on workability, early age hydration, microstructure, mechanical and transport properties was determined. Different characteristics of GO and rGO such as molecular structure, functional groups, ***d*** spacing, size and physical strength influenced the properties of the cement based composites. The workability and final setting time of composite gradually decreased compared to 100% PC (control) with higher dosages of GO up to 0.06 wt% (of cement), which is due to the dominant oxygen functional groups and the hydrophilic nature of GO. To the contrary, the workability and final setting time increased in the rGO composites compared to the control mix due to the almost hydrophobic nature of rGO and the presence of superplasticiser. The XRD and TGA quantification of the hydration products shows that GO composites have a greater content of $Ca(OH)_2$ and C-S-H compared to rGO composites measured at 1, 7 and 28 days. Micropores (smaller than ~ 10 µm) in GO composites were observed to be filled with calcium silicate hydrate (C-S-H) gel and crystalline compounds. Random pore filling nature was observed in rGO composites and ettringite was more common element in those pores. Meso and gel pores (< 2 nm) related to C-S-H show increasing trend in the GO and rGO composites compared to the control mix in dynamic vapour sorption (DVS) analysis. Compared to the control mix, the 28-day compressive strength increased by

~10% and ~15% in 0.06 wt% of GO and rGO in the composites. However, the highest flexural strength was increased in the 0.04 wt% of GO and 0.06 wt% rGO composite, and the enhancement was 75.7 % and 33.7 %, respectively, compared to the control mix. The electrical resistivity value increased with the incorporation of GO and rGO. The water sorptivity coefficient of 28-day GO and rGO composite reduced 24.8% and 4.7%, respectively, compared to the control mix.

**Keywords:** Graphene oxide (GO), reduced graphene oxide (rGO), nano-cement composite, hydration process, mechanical properties, transport properties, microstructure.

## 1. Introduction and background

Graphene is a nanomaterial with extraordinary physicochemical properties. It is one atomic thick 2D plane layer of hexagonal carbon allotrope with several nanometers (~1-8 nm) thickness compared to its several hundred nanometers (~1,000-100,000 nm) of length [1–10]. There are different forms of graphene materials which vary in chemical compositions, physical properties and morphology. The chemical oxidation and exfoliation of graphite (chemical reduction route) is the most convenient method for producing bulk quantity (kilograms) of graphene materials [11], which can yield two primary forms of graphene [9]: graphene oxide (GO), and reduced graphene oxide (rGO). GO is graphene layers with oxygen-containing functional groups on its surface, such as hydroxyl (-OH), epoxide (C-O-C), carboxyl (-COOH), and carbonyl groups (C=O) [12]. Due to these functional groups, GO is amorphous [9], non-conductive, and poses lower physical strength compared to graphene. The functional groups make GO hydrophilic and highly dispersible in water. rGO is produced by reducing the functional groups of GO [5], which partly restores the physical strength and electrical conductivity of graphene layers [9]. The reduction of functional groups from GO to rGO transforms the microstructure and physical properties to be similar to that of graphene, yet, rGO is not completely oxides defect-free graphene and partially dispersible in water.

Microfibers such as steel, glass, polymer and carbon fiber are conventionally used in concrete and cement composite to attain high mechanical and ductile performance. Table 1 presents the physical properties of conventional fibers used in concrete, along with recently developed carbon nanotube,

graphene, GO and rGO materials. The physical properties of graphene are significantly superior compared to other fiber materials; the reported tensile strength and elastic modulus are 130 GPa and 1000 GPa, respectively, for graphene, compared to that of 1.5 GPa and 200 GPa, respectively, for steel fibers. The chemical and electrical properties of different forms of graphene nanomaterials can be designed to serve a specific purpose at the nanoscale [11,13–16]. As such, graphene nanomaterials offers new opportunities to develop further improved cement-based composites [3,5,6,8,9,17–23].

**Table 1.** Physical properties of conventional fibres, graphene, CNTs and GO materials.

| Fiber type | Tensile strength (GPa) | Elastic modulus (GPa) | Elongation at break (%) | Diameter/ thickness (µm) | Aspect ratio | Information source |
|---|---|---|---|---|---|---|
| Steel | 1.5 | 200 | 3.2 | 500 | 20 | Reproduced from [24] |
| Glass (E-glass) | 3.45 | 72 | 4.8 | 5–10 | 600–1500 | |
| Glass (AR-glass) | 1.8–3.5 | 70–76 | 2 | 12 | 600–1500 | |
| Polypropylene | 0.1–0.8 | 8 | 8.1 | 100 | 150 | |
| Polyvinyl alcohol | 0.8 | 29–36 | 5.7 | 14–650 | 430–860 | |
| Carbon | 2.5 | 240 | 1.4 | 7 | 710 | |
| Graphene | ~130 | 1000 | 0.8 | ~0.08 | 6000–600,000 | [25,26] |
| CNTs | 11–63 | 950 | 12 | 15–40 | 1000–10,000 | |
| GO | ~0.13 | 23–42 | 0.6 | ~0.67 | 1500–45,000 | |
| rGO | unknown | 250±150 | unknown | ~0.08 | unknown | [27] |

*GO: graphene oxide, rGO: reduced graphene oxide, and CNTs: carbon nanotubes

The distinctive hydrophilic and water dispersibility nature of GO is favourable for its incorporation into cement to form a uniform composite. This is the primary reason why most of the existing studies prefer to use GO to improve the mechanical properties and durability performance of the cement-based composites [3,6,17–23]. On the other hand, limited studies have been conducted on rGO cement-based composites [5,8,9].

Studies reported that GO and rGO influence the cement hydration processes [3,5,9,17–20,28]. However, the influence of GO and rGO on the cement hydration process is poorly understood, with different researchers expressing different opinions. According to Horszczaruk et al. [18], the kinetics of the cement hydration process is not strongly influenced by the GO that they studied which has a thickness of 0.86 nm. To the contrary, GO has also been reported to accelerate the degree of hydration of Portland cement (PC) paste systems [19]. Lv et al. [3] claim that GO (oxygen 29.75%, thickness 8 nm and size, i.e. length or width of 2D plane 80-260 nm) regulates the formation of flower-like

hydration crystals that substantially improve the mechanical strength of the composite. However, Cui et al. [20] contradict these findings, particularly due to the scanning electron microscopy (SEM) sample preparation method, because the flower-like crystals are the carbonation products of the cementitious hydrates. A recent study suggests that the functional group's reduction level in rGO from GO significantly varies 28 days cement composite degree of hydration in the rage of ~16.5-22.5% [9]. This could be due to the effects of functional groups on the characteristics of graphene materials. Therefore, the characteristics of GO and rGO should be explicitly examined and correlated to explain their performance on the cement hydration process.

Both GO and rGO have been reported to influence the pore volume distribution in the cement composite matrix [5,17,19]. GO of varying sizes (1-200 $\mu m^2$) were reported to increase small pores (1-45 nm) in the composite, while the pore volume in the range of 45-80 nm was similar in Portland cement (PC) and the GO-cement composite [17]. Pores smaller than 10 nm diameter are primarily gel pores contained within C-S-H gel. Hence, the higher proportion of gel pores in GO-cement is an indirect indication of higher C-S-H concentration in the GO-cement composite. A composite of GO (with an average dimension of 520 $nm^2$ and an approximate thickness of 1 nm) shows a reduction of approximately 13.5% total porosity and 27.7% capillary pores (10 nm - 10 μm) and over 100% larger amount of gel pores compared to that of 100% cement samples [19]. Micropores (~0.5 μm) in the rGO composite has also been reported to fill with rGO sheets [5]. An increase in the gel pore volume in the composite is an indirect indication of the influence of graphene materials on the cement hydration process.

A wide range of GO dosages (0.01-2.00 wt% of cement) was investigated by different researchers aiming to understand the interplay between GO dosage and the mechanical properties of the cement-based composites [5,6,8,13,21,23,29]. Qiu et al. [23] studied cement composite with 0.02 wt% GO (25.45% oxygen, thickness 15 nm, and size 80-300 nm) and reported improvement in the tensile and flexural strengths by 197.2 and 184.5%, respectively compared to the 100% cement paste. Mokhtar et al. [6] investigated GO (layer thickness < 100 nm and size 1-2 μm) within a range of 0.01 to 0.05 wt% of cement in the paste composite. They reported that 0.02 and 0.03% GO improves tensile and

compressive strengths by about 13 and 41%, respectively, compared to the 100% cement mix. Even though, the compressive strength was reported to decrease with the incorporation of GO from 0.02 to 0.03 wt% of cement; there was an improvement in tensile strength from ~2.8 to 3.8 MPa [6]. The mechanical properties were observed to improve in Qiu et al. [23] compared to Mokhtar et al. [6] despite similar GO dosage, w/b ratio, curing regime and age. A relatively high volume percentage (2 %) of GO (size < 2 μm and thickness 1-5 μm) in cement was reported to have an increased compressive strength and elastic modulus about 54% and 50%, respectively, compared to the 100% cement mix [30]. Another study by Li et al. [21] suggested that the compressive strength of the GO-composites can increase by up to 46.8% compared to the 100% cement paste with the increasing GO (C/O ratio of 1.36-0.98) proportion from 0 to 0.08 wt% of cement. In the same study [21], 0.04 wt% of GO in the composite resulted in 14.2% increment in flexural strength compared to the 100% cement paste.

The addition of 0.02 wt% rGO of cement in the composite increased the flexural strength by 23% compared to the 100% cement paste after 28 days [8]. An in-situ rGO based fly ash cement composite is studied [5], where about 0.35 wt% rGO of cement in the composite increased flexural strength, Young's modulus and flexural toughness by 134%, 376%, and 56%, respectively, compared to the fly ash cement paste without rGO. Nevertheless, the mechanical strength performance of the rGO composite considerably varies with the reduced level of functional groups from GO [9]. Hence, the usage of rGO in the cement based composite should be studied carefully.

The transport properties of the GO and rGO cement composites are reported in limited studies. The ingress of chloride ions hinders in GO mortar composites [22]. The electrical resistivity measurement at early ages i.e. 24 h in the GO-cement composite also reported increased compared to the 100% cement mix [21]. Only one study reported that rGO in the composite decreased mass porosity and water sorptivity in 7 days then increased both in 28 days [8]. So far, there is no study compared the transport properties between the GO and rGO composites.

All these discussed studies on the GO and rGO cement based composite show the potential for improving mechanical properties and microstructure, yet there are existing research gaps. Firstly, critical GO and rGO parameters, such as size, i.e. size (length or width) of 2D plane, layer thickness, numbers of layers, C:O ratio, functional groups, surface chemistry and interlayer distance (***d*** spacing), as well as physical strength need to be correlated with GO and rGO's performance in the cement-based composites. And secondly, hydration kinetics of the GO and rGO cement based composite, and their transport properties required direct comparison with in-depth investigation.

To address these research gaps, the objective of this study is to compare the impact of a highly functionalized form of GO and a highly reduced functional groups containing rGO in the cement based composites. The GO has a C:O ratio of ~54:46, ***d*** spacing of 0.87 nm and size of 1.2±0.8 µm, and the rGO has a C:O ratio of ~82:18, ***d*** spacing of 0.36 nm and size of 17.5±9.2 µm. The critical parameters of GO and rGO were correlated to study their impact in the composite.

## 2. Materials and methods

### 2.1 Materials and characterisation

The graphene nanomaterials (GO and rGO) supplied by Graphenea Inc., Cambridge, USA and their properties are presented in Table 2 as per the production data sheet and microstructural measurements by the authors. Microstructural investigation was carried out by X-ray diffraction (XRD), Fourier-transform infrared spectroscopy (FTIR), Raman spectroscopy, optical microscope, SEM, and Energy dispersive X-ray (EDX) observation. It could be noted that critical parameters i. e. C:O ratio, ***d*** spacing and mean size of GO are higher than rGO. General use cement supplied by CRH Mississauga plant in Canada was used in this study, and its chemical composition is shown in Table 3.

**Table 2.** Physical properties and elemental composition of GO and rGO.

| | Physical properties | | | | | Elemental composition (%) | | | | |
|---|---|---|---|---|---|---|---|---|---|---|
| | Mean size | ***d*** spacing | Layer thickness | Surface area | Electrical conductivity | C | H | N | S | O |
| GO | ~ 1 µm (1.2±0.8 µm[***]) | 0.87 nm | 1-2 nm | Not measured | Not applicable | 49-56 | 0-1 | 0-1 | 2-4 | 41-50 |

| | | | | | | | | | | |
|---|---|---|---|---|---|---|---|---|---|---|
| rGO | 0.26-0.30 µm* (17.5±9.2 µm***) | 0.36 nm | 1 nm | 422.69-499.85 $m^2/g$ | ~667 S/m** | 77-87 | 0-1 | 0-1 | 0 | 13-22 |

* Measurement in terms of zeta-sizer in NMP (N-methyl-2-pyrrolidone) at 0,1 mg/mL.** Measured in a 20 nm thickness film. ***Particle size measurement form SEM image analysis enclosed in Appendix-A.

**Table 3.** The chemical composition of general use cement in percentage.

| $SiO_2$ | $Al_2O_3$ | $Fe_2O_3$ | CaO | MgO | $SO_3$ | Total Alkali | Free Lime | LOI |
|---|---|---|---|---|---|---|---|---|
| 19.3 | 5.50 | 2.70 | 61.20 | 2.60 | 4.00 | 0.92 | 0.60 | 2.50 |

GO was received as 4 mg/mL dispersion in water whereas rGO was received as a dry powder. Fig. 1 presents the molecular structure and microstructural characterisation results of GO and rGO. The molecular structure shows the lower content of functional groups present in rGO compared to GO (Fig. 1a, b). The XRD was measured using a Philips PW 3710 X-ray diffractometer with a Cu-$K_\alpha$ radiation source and 2θ in the range of 5-60$^o$. Measurements were performed at 2 s per scan on a zero XRD background silicon screen. The XRD pattern shows a major diffraction peak at 2θ ~10.12$^o$ for GO, and 2θ ~24.90$^o$ and 43.18$^o$ for rGO (Fig. 1c). The diffraction peak for rGO at 2θ ~43.18$^o$, indicated a short-range order in rGO stacked graphene layers. Similar XRD patterns for GO and rGO were reported in [31]. The interlayer distance (***d*** spacing) between graphene layers for GO and rGO calculated using the Bragg's equation are ~0.87 nm and ~0.36 nm, respectively. The interlayer distance increases with the oxidation of graphite to form GO, then the reduction of functional groups from GO to rGO reduce it again. Thermo Scientific iS50 FTIR was used to investigate the vibrational stretching modes of different molecular bonds to compare the changes of the oxygen functional groups between GO and rGO. FTIR graph is presented in Fig. 1d. GO shows the bond stretching peaks for hydroxyl (-O-H at ~3220 $cm^{-1}$), carbonyl (C=O at 1730 $cm^{-1}$), aromatic (C=C at 1620 $cm^{-1}$), carboxy ( C-O at 1415 $cm^{-1}$), epoxy ( C-O-C at 1228 $cm^{-1}$), hydroxyl ( C-OH at 1070 $cm^{-1}$). In comparison, rGO demonstrated substantial losses of oxygen functional groups, in particular, hydroxyl and epoxy groups. The remaining peaks are mainly aromatic benzene C=C bond stretching and a minor stretching for carboxyl groups, which indicates a highly reduced state of rGO. The infrared patterns are all in agreement with those reported in previous studies [9]. A Bruker SENTERRA dispersive Raman microscope was used for scanning both GO and rGO at 532 nm wavelength. Fig. 1e

shows typical D and G Raman bands of GO and rGO, which are located at ~1350 $cm^{-1}$ and ~1583 $cm^{-1}$, respectively. The ratio between this D and G Raman bands intensity, $I_D/I_G$, is an efficient indicator for determining the level of functional groups presence in GO and rGO. The intensity ratio ($I_D/I_G$) is about 0.87 for GO, while the intensity ratio of rGO is much higher (1.14). The higher intensity ratio 1.14 of rGO implies that the oxygen functional groups were significantly reduced compared to GO. The increase of the $I_D/I_G$ intensity ratio from GO to rGO is related to the removal of functional groups and the formation of defects. This observation is consistent with the literature [32,33] and correspond to the findings of this XRD and FT-IR.

Both GO, and rGO were dispersed in water prior to mixing with cement. GO was dispersed in water in two steps: i) GO (4mg/mL) was mixed with tap water using a magnetic stirrer for 2 h at 1000 rpm, ii) the solution was sonicated using a 40 KHz bath sonicator (Branson 5510) for 3 h. The dispersion of rGO in water was conducted in four steps: (i) rGO powder was carefully collected in 10 ml deionized water in a fume hood, ii) rGO-deionized water mix was added to 1490 ml tap water with 0.4% superplasticiser (Polycarboxylate, Plastol 6400 supplied by Euclid Canada) and mixed for 3 hr at 1000 rpm, iii) the mixture was sonicated for 3 h, and iv) the rGO solution was stirred for an additional hour prior to the casting of the composite. The dispersion of GO and rGO in water was observed by optical and SEM microscope imaging (Fig. 1f-i). The rGO was agglomerated in micro thin planes (Fig. 1 g and i); whereas GO forms uniform thin planes (Fig. 1 f and h) homogeneously dispersed in water. The rGO dispersion nature in water is similar to graphene. Graphene readily agglomerates in polar solvents due to its hydrophobic nature [1], which was similarly observed for rGO in water. The SEM images also show uniform thin plane formation pattern by GO compared to rGO (Fig. 1h, i). The average C:O ratio of GO and rGO according to EDX was 54:46 and 82:18, respectively after dispersion. The EDX quantification is a close approximate approach owing to the quantification of a spot where the electron beam of SEM is falling. Similar C and O content measurement using energy-dispersive X-ray spectrometer (EDS) was reported in the literature Lv etal. [3] and Qiu etal. [23]. In addition, the EDX quantification of C and O elemental composition falls within the range of materials data sheet information provided by Graphenea Inc. and presented in Table 2.

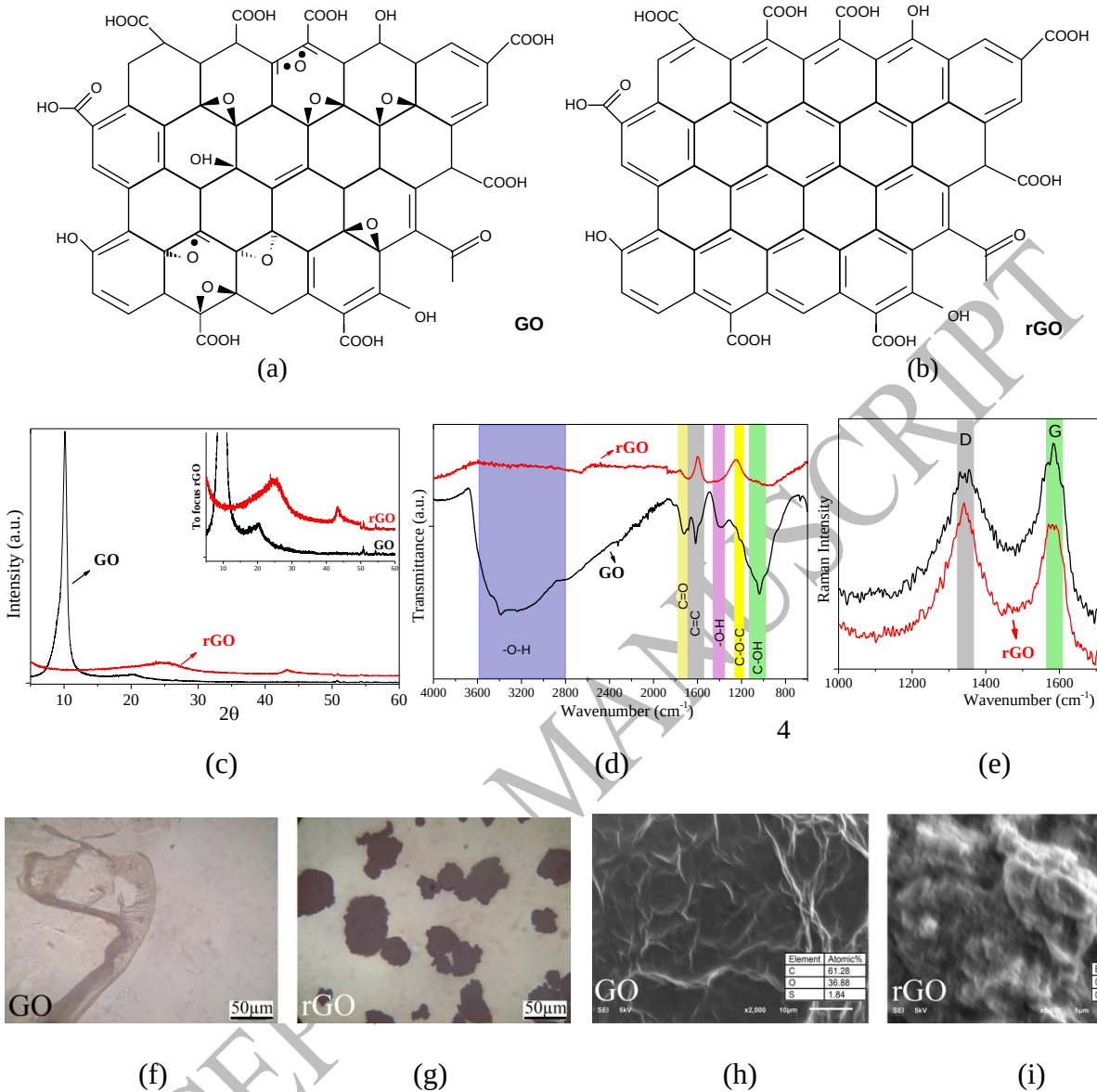


**Fig. 1.** Characterisation of as received GO and rGO: (a) GO structure, (b) rGO structure, (c) XRD pattern of GO and rGO, (d) FTIR pattern of GO and rGO, (e) Raman pattern of GO and rGO, (f) light microscope image of GO dispersion in water, (g) light microscope image of rGO dispersion in water, (h) SEM image of GO layers and (i) SEM image of rGO layers.

## 2.2 Preparation of cement paste composite

Seven batches of cement paste composite were prepared based on mix proportions detailed in Table 4. The water to cement ratio (w/c) of 0.45 was preferred to achieve efficient dispersion and uniform

mixing of both GO and rGO in the cement composite systems. The composites were cast and finished as prescribed at BS EN 196-1:2005 [34] using a planetary type mixture. First, the water, or GO, or rGO solution was pour in the bowl and premixed at 140 rpm for 15 s. The cement was then mixed for 30 s, and the mixing speed was increased to 285 rpm and continued for 60 s. The mixing was stopped for 60 s while the paste collected on the side of the container was scraped down into the hatch. Finally, the mixing continued at 285 rpm for 30 s, stopped for 15 s and then started again at the same speed for 30 s.

For each batch, nine cubes (50x50x50 mm), three cylinders (50 mm diameter x 100 mm height) and six prisms (25x25x100 mm) were prepared. After casting, the samples were stored at a relative humidity > 90% and a temperature of 23±1 $^{o}$C. Specimens were demoulded after 24 hr and submerged in water at a temperature of 23±1 $^{o}$C.

**Table 4.** Mix proportions of GO and rGO paste composite.

| Mix ID | Water/PC (by weight) | GO (wt.% of cement) | rGO (wt.% of cement) |
|---|---|---|---|
| 0% Control | 0.45 | - | - |
| 0.02% GO | 0.45 | 0.02 | - |
| 0.02% rGO | 0.45 | - | 0.02 |
| 0.04% GO | 0.45 | 0.04 | - |
| 0.04% rGO | 0.45 | - | 0.04 |
| 0.06% GO | 0.45 | 0.06 | - |
| 0.06% rGO | 0.45 | - | 0.06 |

## 2.3 Testing procedure

A mini-slump test was conducted just after mixing, and the paste sample was tested for calorimetric analysis. Microstructural analysis was conducted to understand the hydration process of composites based on TGA and XRD on 1, 7 and 28 days sample, as well as SEM and EDX on the 28 day sample. The mechanical performance was assessed based on compressive strength and flexural strength tests. Finally, electric resistivity up to 28 days and water sorptivity tests on 28 days sample were performed to study the transport properties.

### 2.3.1 Measurement of workability

The workability of composites was assessed using a mini-slump test. A mini cone mould of the following dimensions: top diameter 19 mm, bottom diameter 38 mm, and a height of 57 mm was used in this slump test. The measuring procedure was adopted from [35] to determine the static flow diameter. The cone was placed on a plastic sheet and filled with paste compacted ~ 15 times with a spatula. Then the cone was lifted vertically, and the flowed slump paste was left to set over 24 h. The average slump diameter was based on three measurements. The dynamic flow of the composite paste was assessed according to ASTM C1437-07 [36]. However, there was one modification, the table was raised and dropped 15 times in about 9 s whereas the standard specifies 25 times in 15 s. The reason for this modification is that some mixes may tend to spread more than the diameter of the table (~25 cm), and the purpose of the test would be lost. The flow diameter was determined by averaging two diameters of slump perpendicular to each other.

### 2.3.2 Characterisation of hydration and microstructure

The calorimetric study was conducted on ~6 g samples using a thermometric TAM air calorimeter. The calorimeter began to record heat release data after the cement was in contact with water or graphene solution for about 6±1 min. The heat released from the hydration was monitored every 60 s for 48 h and the data measured was normalised by sample mass.

The microstructure of composites was analysed using TGA, XRD, SEM, and EDX. The sample for analysis was collected from cutting the prisms at 1, 7 and 28 days. After collection, samples were immediately treated with acetone for about 2-3 h to restrict hydration. For TGA and XRD, samples were ground to pass 45 μm mesh sieve and treated with acetone for 2 days flowing vacuum oven drying for another 2 days at 38 $^{o}$C and put into vacuum desiccator with silica gel for 1 more day prior testing. The $Ca(OH)_2$, i.e. CH content was measured by TGA using a Netzsch thermische analyse STA 409 cell. The test was started at room temperature ~25 $^{o}$C and increased to 1000 $^{o}$C over 1 h 42 m. The XRD was measured using a Philips PW 3710 x-ray diffractometer with a Cu-$K_\alpha$ radiation

source. The diffractometer was operating at 30 kV and 40 mA, and emitting radiation at a wavelength of 1.5405 Å. The scanning ranged between 5-70$^{o}$ of 2θ at a rate of 1.25 s/step and a scanning resolution of 0.02 $^{o}$/step. Following the scanning, the raw diffraction data was located in the PDF-2004 database using X'pert Highscore software to identify peaks in the XRD pattern, and phase quantification was conducted using Rietveld analysis. The SEM imaging and EDX elemental measurement were carried out on 28 days samples, using a JEOL JSM-6610LV SEM machine and an X-Max Oxford EDX detector type.

The DVS was also used to investigate the meso and gel pore structure of the cement paste. The measurement was taken using a DVS Advantage 1 machine supplied by Surface Measurement Systems, London, UK. Approximately 10 mg of dry powder sample was taken from the samples that were prepared for the XRD and TGA analysis. Samples were placed on the dish in the DVS chamber for vapour absorption measurement with high precision. The relative humidity (RH) mixing with nitrogen gas was automatically controlled at 25 $^{o}$C constant temperature in the DVS chamber. A single sorption cycle consisting of adsorption up to 98% RH followed by desorption back to 0% RH was run for the pore structure analysis. The specific surface area of the inner pore area was calculated using Brunauer Emmett Teller (BET) method from the adsorption branch of isotherm. The pore size distribution up to 22 nm was calculated using the Barrett, Joyner, and Halenda (BJH) method. The BET and BJH method calculation process are followed as described in [37].

**2.3.3 Mechanical strength test**

The mechanical properties that were tested are compressive strength and flexural strength. Three samples were tested for each property to report the mean and standard deviation. The compressive strength test was performed on 50 mm cubes according to ASTM C109 [38] using a Forney 440 kN compression testing machine at a loading rate of ~2.4 kN/s. The flexural strength test on prisms (25x25x100 mm) was performed on Autograph AG-I, Shimadzu 50 kN testing machine following ASTM C348 [39]. The displacement rate was 0.1 mm/min, and the span length was 75 mm.

### 2.3.4 Transport property tests

Electrical resistivity and water sorptivity test were performed to analyse the transport properties in the composites as an indication of durability performance. The electrical resistivity was measured on 50 mm cubes according to the uniaxial two-electrode method described in [40,41] and using a GIATEC Scientific RCON concrete resistivity meter. Two parallel metal plates with moist sponges were contacted at the opposite surface of cube specimen, and the drop in the potential between two electrodes was measured while an AC current was applied at 1 kHz frequency. The electrical resistivity of the composites was monitored from 1 day to 28 days. Electrical resistivity is related to composite density as such higher the resistivity denser is the matrix; then again electrically conductive materials may have a different impact on the composite electrical resistivity. A liquid capillary sorptivity test was performed on 50 mm cubes following [42] and detail procedure described in [43]. Cube samples were cured for 28 days, then the surface of the sample was cleaned and put into a dry vacuum desiccator with silica gel (3-5 days) at a temperature of 23±1 $^{o}$C until the mass changes were 0.1% in a 24 h period. Cubes were then wrapped around four sides with aluminium tape keeping two opposite surfaces open to prevent water penetration from the sides during sorptivity. The cubes were then placed into a water bath facing one open side maintaining a water level of ~1.5 mm.

## 3. Results and discussion

### 3.1 Workability

The static and dynamic flow diameters resulted in mini-slump test are presented in Fig. 2. Both the static and dynamic flow diameters were reduced approximately 29% and 16%, respectively in the 0.06% GO composite, compared to the control mix (0% GO ro rGO). The flow diameter reduces with the increasing proportions of GO, which indicates that the loss of workability is proportional to the percentage of GO in the composite paste. This is due to the hydrophilic high specific surface area and

high interlayer distance (0.87 nm) of GO nanomaterials 2D plane which requires extra water to wet their surface. Hence, some researchers were using superplasticisers to improve the workability of GO cement based composites [28,30]. The static and dynamic flow diameter in the rGO composites increased approximately 95% and 24 %, respectively, compared to control. Superplasticiser was used in rGO solution for an efficient dispersion which has improved the workability similarly in all the rGO composites. Also rGO has minimum impact on the workability of the composites. rGO does not extract extra water from the composite since this rGO is almost hydrophobic with a low interlayer distance (0.36 nm).

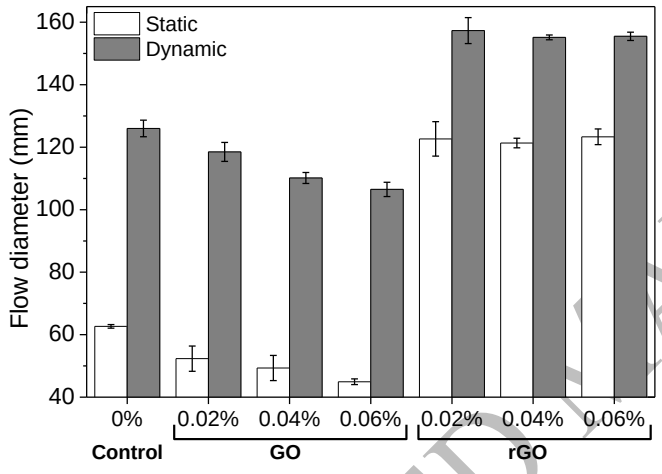


**Fig. 2.** Static and dynamic flow diameter in the mini-slump test.

### 3.2 Cement hydration process and microstructural development

Calorimetric study on early age (first 48 h) paste samples, TGA and XRD on 1, 7, 28 days samples, and SEM-EDX on 28 days samples were undertaken in this study, to analyse the impact of GO and rGO in the cement hydration process and the development of microstructure.

#### 3.2.1 Early age hydration kinetics

The rate and cumulative heat of hydration of the control and composite pastes recorded by the calorimeter are shown in Fig. 3. Both the GO and rGO paste composites exhibited a higher rate of heat of hydration and cumulative heat compared to the control paste. While comparing the GO and

rGO impact on heat release, both the rate and cumulative heat of hydration were higher for the rGO composites than the GO composites.

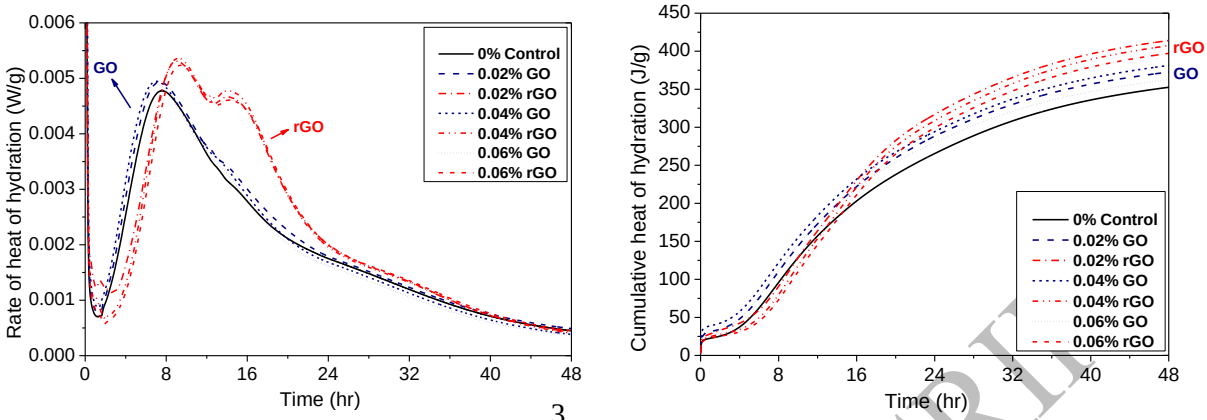


3

(a) (b)

**Fig. 3.** Effect of GO and rGO on the hydration heat release of composite pastes during 48 h hydration: (a) rate of heat of hydration over time, (b) cumulative heat of hydration over time.

Typically two peaks generate in the rate of heat of hydration curve (Fig. 3a). The first peak evolves due to the hydration of $C_3S$ and indicates the final setting time, whereas the second peak corresponds to the hydration of $C_3A$ phase of cement. These peaks of the heat flow increased and shifted to the left in the GO composites and to the right in the rGO composites compared to the control mix. The trend of the cumulative heat of hydration after 48 h for GO composites stands as 0.04% GO > 0.02% GO > 0.06% GO > control, and for rGO composites stands as 0.02% rGO > 0.04% rGO > 0.06% rGO > control.

Within the first 24h, GO has accelerated the hydration process of cement through enhanced nucleation facilitated by its large surface area and active oxide functional groups [21,28]. The final setting time in the GO composites reduced about an hour through this process compared to the control mix. The rGO, on the other hand, delayed the appearance of both peaks in the rate of heat of hydration curve, and the magnitude of the rate of heat and cumulative heat were increased significantly compared to the control mix. The shift corresponds over an hour delay in final setting time which may be the effect of superplasticiser in the rGO dispersed water. However, the increment in the heat of hydration magnitude is due to the active participation of rGO in the cement hydration process. During the first

12 h of hydration, the rGO composite exhibited lower cumulative heat release than that of the GO composite and the control mix, which may be due to the dilution effect of rGO content in water dispersion (Fig. 3b). Typically the second peak corresponds to the $C_3A$ hydration to from further ettringite which appears around 15 h. The cumulative heat release between 12 h and 16 h, altered in the rGO composites and increased compared to the GO composites and the control mix. This implies that rGO plays a major role in the $C_3A$ hydration process.

### 3.2.2 Thermogravimetric analysis (TGA)

The TGA weight loss, a derivative of TG (DTG) and the mass loss for $Ca(OH)_2$ decomposition analysis results are presented in Fig. 4. The weight loss percentage gradually decreases with the increasing temperature and the DTG presented inflections corresponds to the specific phase of compounds decomposition. The TGA provided the content of $Ca(OH)_2$, which reflected the degree of hydration of the corresponding hydrated cement composite. The endotherms and their corresponding mass losses in Fig. 4a were similar to other studies [7,44] and ascribed to ~30-105 $^oC$: the evaporable water and part of the bound water escapes; ~110-250 $^oC$: C-S-H, $C_2ASH_8$, Ettringite, $AFm_{ss}$, mono-carbonate; ~400-500 $^oC$: dihydroxylation of the $Ca(OH)_2$, i. e. CH; ~650-800 $^oC$: decarbonation of calcium carbonate. The degree of hydration of the cement composite is directly correlated to CH content (CH%) which was measured using the following equation:

$$CH\% = (M_{CH}/M_{500}) \times (74/18) \times 100\ (\%)$$

Where, $M_{CH}$ = the percentage weight loss of calcium hydroxide (CH: 400-500 $^oC$), $M_{500}$ = weight at 500 $^oC$, and the fraction 74/18 is used to convert the CH bound water into the CH mass where 74 is the molar mass of $Ca(OH)_2$ and 18 is the molar mass of $H_2O$.

Fig. 4b presents the CH content (%) as a function of GO or rGO content, and time (1, 7, and 28 days). It could be noted that the GO composites resulted in more mass loss for CH than the rGO composites followed by the control mix. The CH mass loss and variation among the GO composites, the rGO composites and the control mix were increasing in 7 and 28 days. Overall, the CH content showed an increasing trend with the increase in both GO and rGO quantity in the composite. The CH content of

28 days indicated that GO composites showed a higher degree of hydration than the rGO composite followed by the control samples. At the 24 h of hydration, both the GO and rGO have accelerated the cement composite hydration process encouraging the nucleation process as increased heat flow resulted in the calorimetric study. This resulted in the production of higher CH content in the composites at 1 and 7 days. Then again, the hydrophilic nature of GO allows it to absorb an additional amount of water molecules on its surface [7,45] and the interlayer, which in the long run (after 7days) may release the free water content required for further hydration. This additional hydration further increased the content of CH at 28 days.

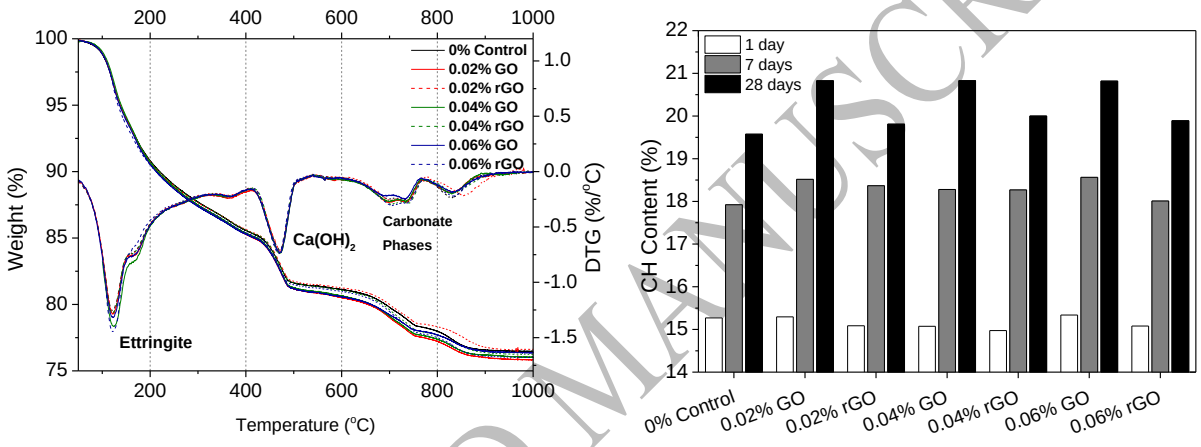


(a) (b)

**Fig. 4.** Thermogravimetric analysis on composite: (a) the TGA and DTG test results at 28 days samples; (b) percentage mass loss for CH phase between 400 °C to 500 °C over time.

In the case of rGO composites, nanomaterials started to impact the cement hydration process a few hours later than GO as indicated in calorimetric heat release study. The lower content of rGO oxygen functional group, rGO agglomeration and superplasticiser delayed cement hydration. However, the almost hydrophobic nature of rGO and the use of superplasticiser in the solution may have increased available water content for efficient hydration in the composite, which ultimately involved rGO in the nucleation and growth stage of cement hydration.

### 3.2.3 X-ray Diffraction (XRD)

The XRD patterns of the cement composites at 1, 7 and 28 days are presented in Fig. 5a-c. Typical cement hydration products such as ettringite, portlandite, i.e. CH, tricalcium silicate ($C_3S$), dicalcium silicate ($C_2S$) detected at all ages. The XRD further verified the results of hydration phases indicated by TGA. The intensity of CH phases increases with increasing content of GO and rGO in the composites and with age. The intensity of the ettringite phases diminishes with the age of hydration and show stronger intensity in the rGO composites. The crystalline phases also increase with the GO and rGO content. Since XRD cannot directly detect amorphous phases, a quantitative analysis using Rietveld software was conducted on the 28 days hydrated composites to quantify the content of amorphous C-S-H gel and other hydration products.

The Rietveld quantification suggests that GO and rGO increased the formation of portlandite (CH) and amorphous (C-S-H) gel phases (Fig. 5d). Compared to the control specimens, the optimum increment of CH content was about 3.5 and 2.7%, respectively in the 0.06% GO and 0.06% rGO composites, and the C-S-H content was about 5.3 and 3.5%, respectively in the 0.02% GO and 0.02% rGO composites. GO increased higher content of CH and C-S-H in the composite compared to rGO. This result is due to the efficient dispersion and active participation of GO functional groups compared to rGO, which is in agreement with the TGA findings.

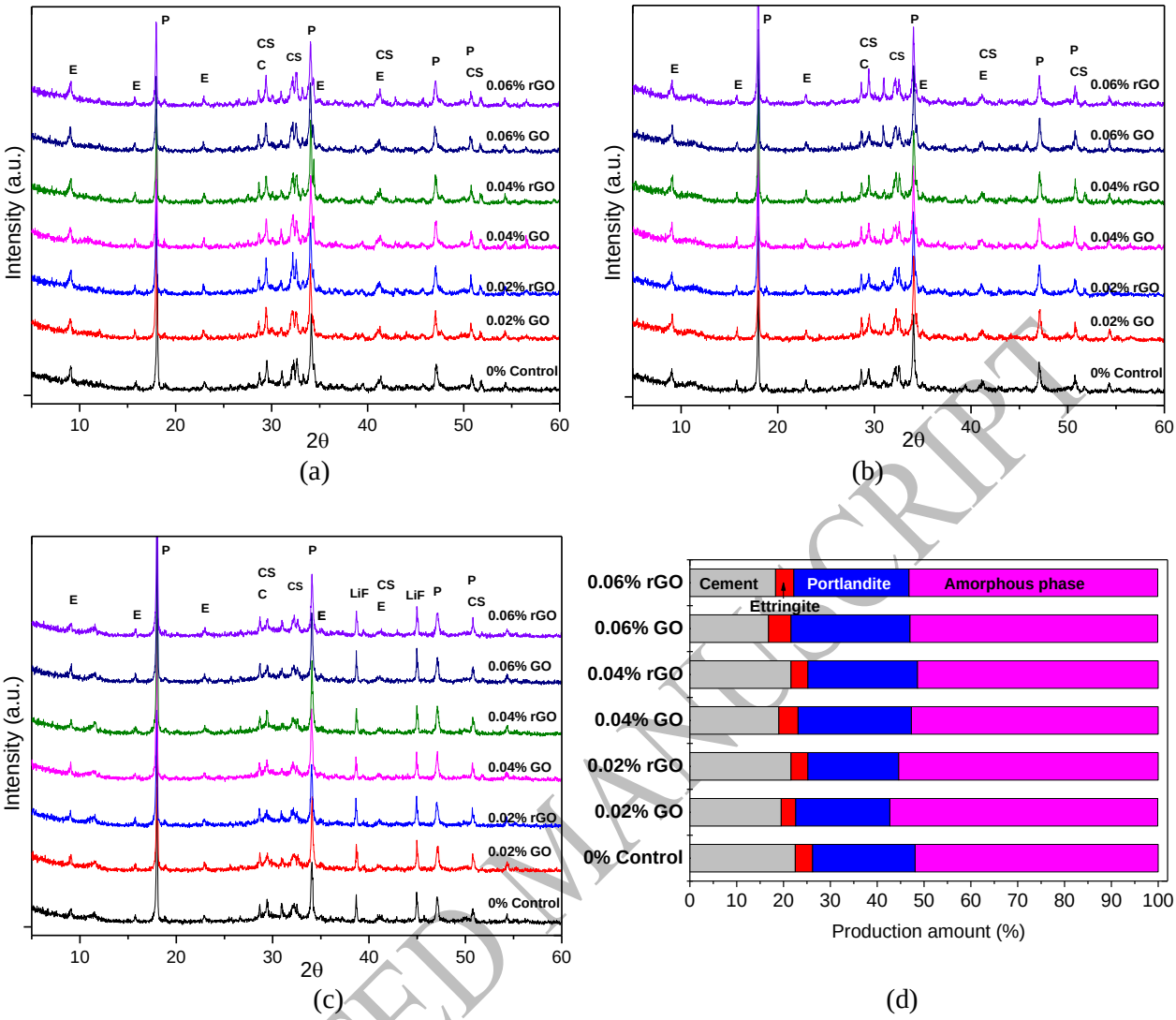


**Fig. 5.** XRD curves of samples: (a) after 24 hr hydration, (b) after 7 days, and (c) after 28 days. Graph notations: E= Ettringite, C= Calcite, CS= $C_2S$ and $C_3S$, P= Portlandite, LiF= Lithium fluoride), and (d) theoretical volume estimated by Rietveld method at 28 days hydrated samples.

### 3.2.4 Microstructural image analysis

The SEM-EDX investigation confirmed the pore filling nature of the GO composites. An ~200 µm pore in the 0.06% GO sample was partially filled with plate-like microstructure together with ettringite (Fig. 6a and b). The EDX detected the presence of calcium and carbon in this plate-like microstructure while it confirms the presence of calcium, aluminium, sulphur and oxygen in ettringite. The micropores of ~10 µm filled entirely in a 0.02 and 0.04% GO sample (Fig. 6c and d) indicating that smaller pores fill efficiently with GO accelerated amorphous C-S-H and crystalline materials.

High dispersibility in water and small plane size (1.2±0.8 μm) of GO encouraged the pore filling performance.

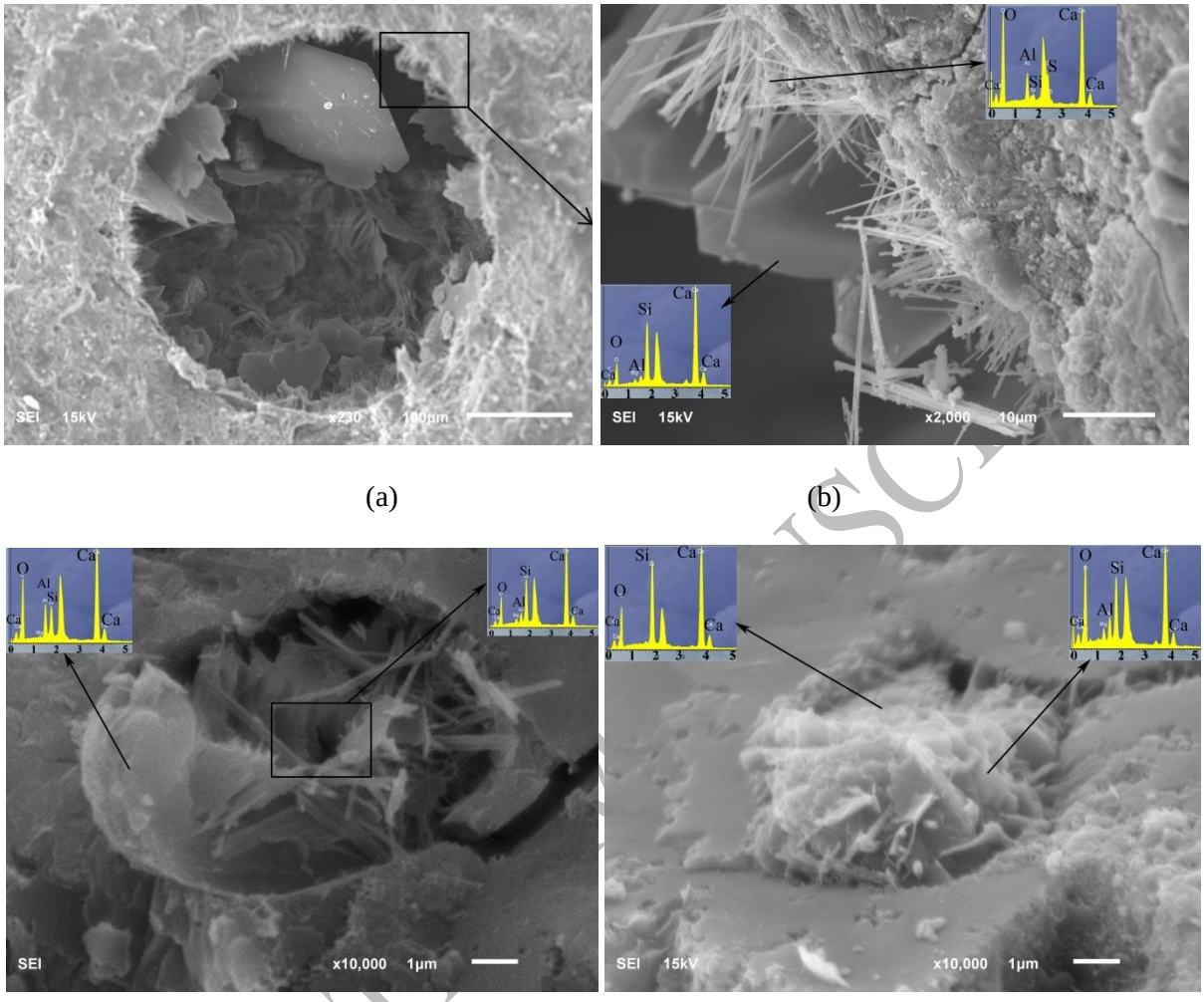


(a) (b)

(c) (d)

**Fig. 6.** The microstructure of GO composite pores: (a) a large pore in 0.06% GO composite, (b) magnification of 'a' indicating the surface growth nature of flake structures and ettringite, (c) a small pore of 0.02% GO and (d) a small pore of 0.04% GO.

The microstructures of rGO composites are denser than the control specimens, and there are indications of microcrack bridging (Fig. 7). However, it is tricky to distinguish the morphology of the rGO layer structure embedded in the compacted cement hydration products such as ettringite, portlandite and C-S-H microstructure in the SEM images because of the formation of those hydration products in rGO surface. Micropores in the rGO composites were filled randomly, and common hydration products were mostly ettringite with partial portlandite and other hydration products.

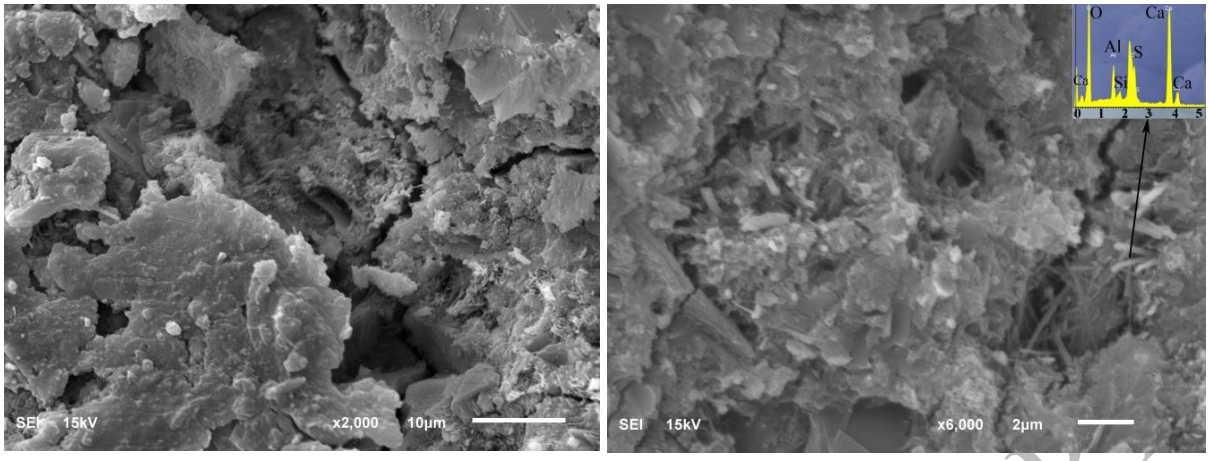


(a) (b)

**Fig. 7.** SEM images of surface: (a) Control (pure cement paste) samples, and (b) Microstructure characteristics in 0.06% rGO.

The SEM and EDX investigations suggest that GO and rGO have good compatibility with the cement hydration products and reinforce the microstructure of composites. The GO and rGO accelerated cement hydration encouraging nucleation on the nano plane surface with oxide functional groups. The functional groups such as carboxylic acid of GO and rGO reacts with cement hydration products, such as C-S-H and CH, and form a strong covalent bond between the cement hydration products, and the surface of GO and rGO. This makes it difficult to identify and quantify a pure state of GO and rGO in the composite matrix. The formation of hybrid materials through the chemical reactions between the carboxylic acid groups of GO and the C-S-H or CH are also reported in similar studies [7,10,17,28,46]. The efficient dispersion of GO and higher content of active hydroxyl and carboxyl functional groups causes a higher rate of C-S-H and CH production with a uniform distribution in the matrix, which may be limited in the rGO composite. The GO composites were commonly filled with C-S-H gel, and a combination of portlandite and calcium aluminosilicate hydrate. The rGO agglomerates in water due to Van der Waals force which was reflected in the composite microstructure as needle-like crystal prone zones (Fig. 7b). Also, high plane size (17.5±9.2 µm) of rGO limits the small micropore (<10 µm) filling performance. Hence, the pores in the rGO composites randomly filled with products such as ettringite and portlandite, while pore filling nature

in the GO composite is more homogeneous. This may lead to a more porous microstructure of the rGO composite compared to the GO composites.

### 3.2.5 DVS pore structure analysis

The DVS sorption isotherms of the graphene cement composite are presented in Fig. 8. The GO and rGO composite have higher water absorption at the target RH of 98%, compared to the control mix. Increasing proportions of GO and rGO in the composite slightly increases the water vapour uptake. In addition, GO composites have slightly high water vapour uptake compared to the rGO composite. The maximum water vapour adsorption at 98% RH increased up to 2% and 1.6% in the 0.06% GO and 0.06% rGO composite, respectively, compared to the control mix. A larger water adsorption means a higher content of C-S-H in the cement paste composite [47]. A higher nucleation and growth rate by GO and rGO in the cement hydration process may have increased the C-S-H gel production. This result is in an agreement with the TGA, XRD and microstructural image invitation results.

Fig. 9 shows the pore size distribution of composites in the range of 0.6-22 nm based on the BJH calculation. The pore size lower than 2 nm radius are related to C-S-H and other refined gel pore structures [37]. The pore volume (< 2 nm) slightly increases with the increase in GO and rGO content in the composite. This implies that GO and rGO composite have higher content of C-S-H gel pore structures than the control mix.

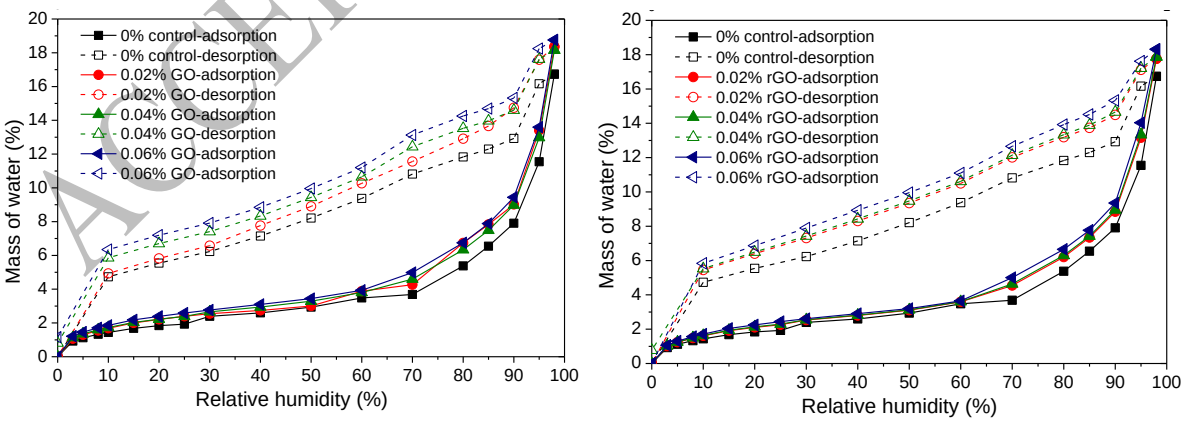


(a) (b)

**Fig. 8.** DVS adsorption and desortion isotherms: (a) control and GO composites, (b) control and rGO composites.

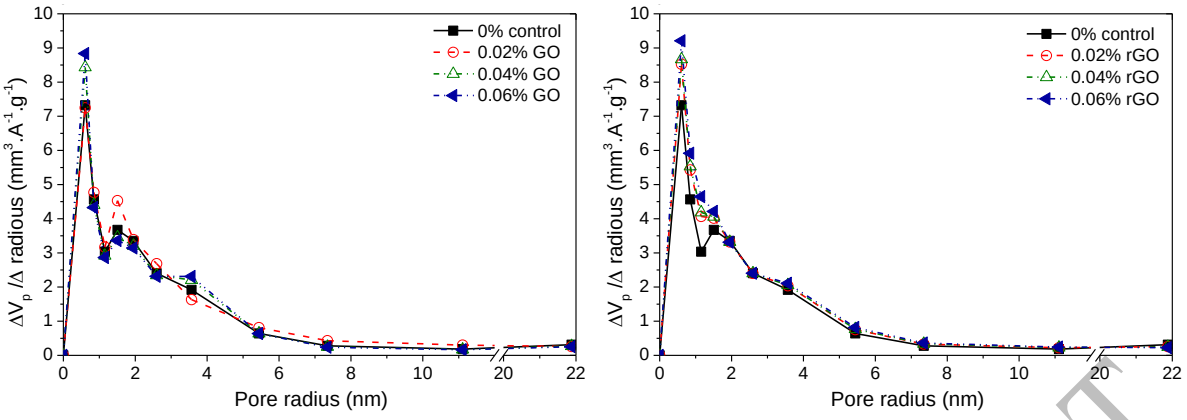


(a) (b)

**Fig. 9.** The BJH method calculated pore size distribution: (a) control and GO composites, (b) control and rGO composites.

The specific surface area were calculated using BET method from the adsorption isotherms (Fig. 8). The specific surface area of paste composite indicates the amount of accessible fine pores. The BET calculated specific area ($A_{BET}$) and total pore volume (Vm) of the composites are reported in Table 5. It could be noteded that GO and rGO increases the the $A_{BET}$ and Vm values compared to the control mix. In a comparison, GO composites have higher $A_{BET}$ and Vm values compared to rGO composites. Increase in specific surface area is related to the increase in the C-S-H content in the GO and rGO composite compared to the control mix as indicated by BJH pore volume distribution and microstructural investigation.

**Table 5.** Specific surface area and total pore volume in the graphene cement composites.

| Range of pore diameter: 0-22 nm | Control | 0.02% GO | 0.04% GO | 0.06% GO | 0.02% rGO | 0.04% rGO | 0.06% rGO |
|---|---|---|---|---|---|---|---|
| Specific surface area ($m^2.g^{-1}$), $A_{BET}$ | 60.45 | 67.41 | 69.31 | 73.11 | 68.68 | 68.56 | 69.80 |
| Total pore volume, Vm ($cm^3.g^{-1}$) | 21.42 | 23.89 | 24.57 | 25.91 | 24.34 | 24.65 | 24.74 |

### 3.3 Mechanical strength of composites

Mechanical strength tests were conducted on the hardened composites and control samples to investigate the impact of cement hydration and microstructure modification by GO and rGO. The compressive strength and flexural strength results are presented in Fig. 10.

Both GO and rGO increased the compressive strength of the composites at 28 days (Fig. 10a). In a quantitative comparison with the control specimen, the compressive strength of the 0.02%, 0.04% and 0.06% GO and rGO composites increased by 10.2%, 7.8% and 10.6%, and 9.6%, 13.3% and 14.9%, respectively. The high content functional groups of GO chemically bonded with cement hydration products and improves the compressive strength. The rGO composites showed a slight increase in compressive strength with the increasing rGO content in the composites due to rGO's high physical strength. Several other researchers [7,48] reported that the compressive strength increment quantity is high in the GO-cement composite compared to 100% cement at an early age (up to 7 days) then the difference in strength increment quantity reduces at a later age (28 days). However, overall compressive strength improvements substantiated that both GO and rGO impacted the cement hydration process.

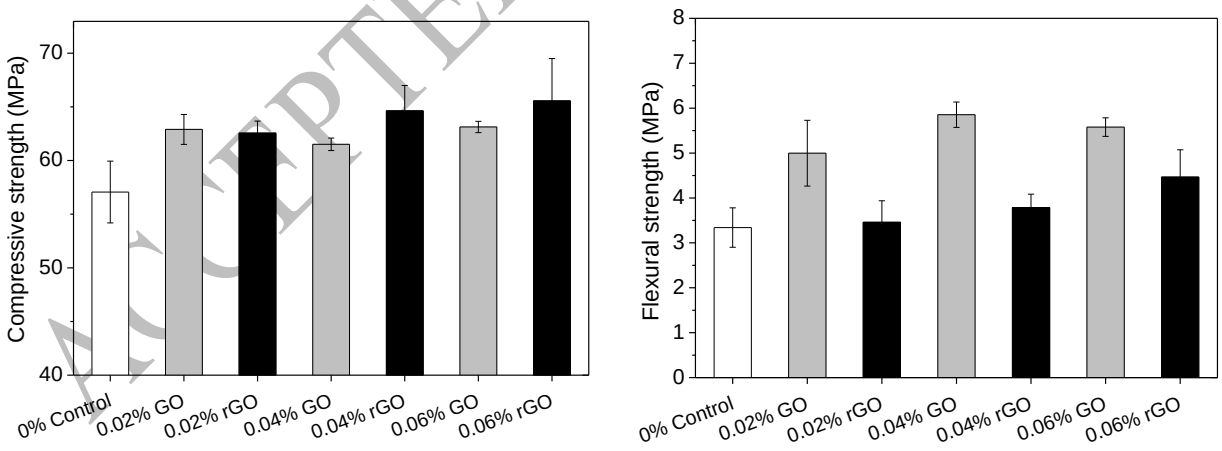


**Fig. 10.** The mechanical strength of different mixes at 28 days: (a) compressive strength, and (b) flexural strength.

In comparison to compressive strength performance, the GO composites show better improvement in the flexural strength than the rGO composites followed by the control mix. For instance, the flexural strength was gradually increasing with the higher content of rGO (Fig. 10b). In a quantitative comparison with the control mix, the 0.04% GO and 0.06% rGO composites resulted in the highest flexural strength increase of 75.3% and 33.7%, respectively. In fact, 0.02% rGO shows similar flexural strength as control, whereas 0.02% GO shows approximately 49.6% increase, compared to the control mix. The GO has more actively participated in the cement hydration process resulting in a denser microstructure compared to rGO. GO contains a higher amount of functional groups both on the surface and periphery of graphene layers that reacts with cement hydration products. This results in a stronger interfacial adhesion bond between GO and the cement matrix. Also, the agglomeration and random pore filling performance of rGO in the composite as evident in SEM images may have restricted the improvement in flexural strength compared to the GO composite despite rGO's superior physical properties close to graphene (Table 1). Therefore, compared to rGO, the higher dispersibility of GO in water together with higher content functional groups participation in chemical bonding with cement hydration products effectively bridged the composite matrix at a nano-micro level. This results in higher flexural strength in GO composites compared to that of the rGO composites followed by the control mix.

### 3.4 Transport properties

#### 3.4.1 Electrical Resistivity

The electrical resistivity was monitored following the demoulding of cube samples from moulds after 24 hr (Fig. 11). The electrical resistivity gradually increases with the hydration time of all mixes. The composites with GO and rGO show higher resistivity than the control mix. The resistivity was found highest in 0.02% dosage of both the GO and rGO composites then it reduces with the increasing GO and rGO content. Although rGO is electrically conductive, the functional groups participate in the cement hydration process which increases C-S-H gel pores in the composite. This increased gel pores lessens mean free paths for the electrons transmission which ultimately increased the electrical

resistivity. In the initial stage, the GO composites show higher resistivity compared to the rGO composites which altered after the first week. This trend correlates with the calorimetric study where the cumulative heat of hydration altered after 12-16 hr. Even with the altering effect by rGO, the later (after 2 weeks) accelerated hydration by GO absorbed water may produce further hydration compounds, which ultimately balances the electrical resistivity performance of GO in comparison to rGO in the composite by 28 days. This is also in agreement with the TGA, XRD, microstructure and DVS results.

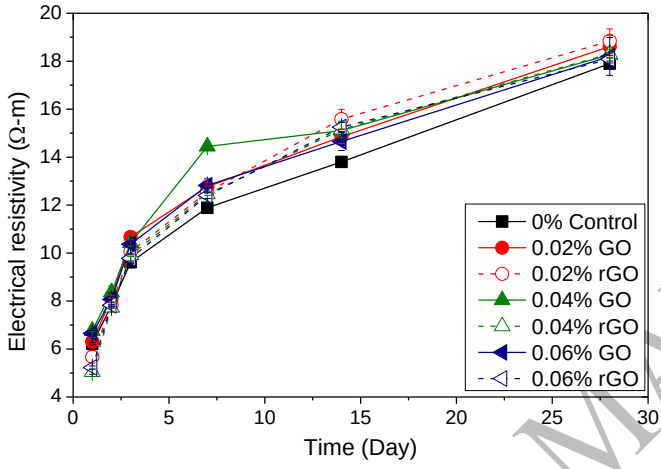


**Fig. 11.** Evolution of electrical resistivity.

### 3.4.2 Water sorptivity performance

Fig. 12 shows the one-dimensional water sorptivity coefficient of the hardened paste composites and the control specimens at 28 days. The sorptivity capacity drops with the higher content of GO and rGO in the composite indicating improvement in the cement composite durability. In comparison, the reduction of sorptivity was more significant in the GO composites than the rGO composites. The sorptivity coefficient of the 0.06% GO and rGO composites reduced by 24.8% and 4.7%, respectively, compared to the control specimen. The densification of the composite matrix by rGO results in a similar sorptivity performance by the 0.02% and 0.04% rGO composite compared to the control specimen. Similar sorptivity results have been reported on rGO cement-based composite by Murugan et al. [8]. Homogeneous C-S-H gel material with the crystalline hydrated compound formation and strong covalent bondage in cement matrix pores by GO may have resulted in this improved sorptivity

performance. In contrast, the rGO composites may have filled porous with ettringite type hydrated compounds randomly while the matrix remains partially porous compared to the GO composites.

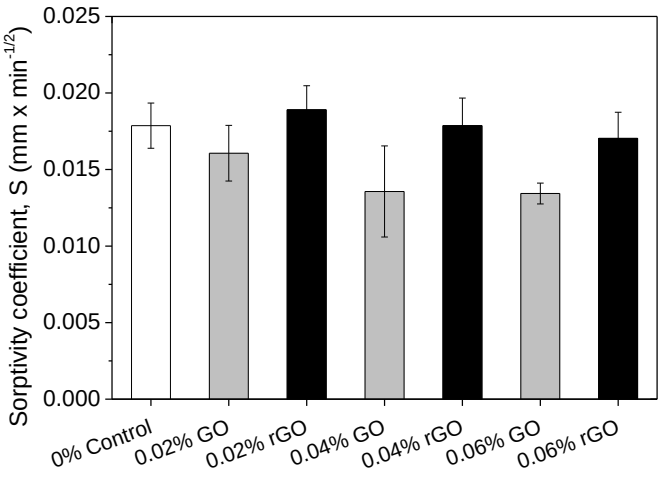


**Fig. 12.** Water sorptivity coefficient at 28 days.

These electrical resistivity and sorptivity results are in agreement with the cement hydration, microstructure characteristics and strength measurements. The efficient dispersions of GO with higher content of functional groups compared to rGO played an essential role in the enhancement of mechanical properties and durability performance. The pore filling materials structure may depend on the active functional groups which dictate the type of cement hydration products formation around the nanomaterials.

## 4. Conclusions

This research examines the workability, hydration, microstructure, mechanical and transport properties of the cement paste composite incorporating two different forms of graphene nanomaterials, GO and rGO at the concentrations of 0.02%, 0.04% and 0.06% by cement weight. The key findings are summarised as follows:

1) The dispersibility, chemical structure, size, interlayer distance, oxygen-containing functional groups and physical strength of GO and rGO were different which dictates the properties of the cement based composites at nano-micro scale.

2) The workability of composites was reduced gradually with the higher percentage of GO since GO is hydrophilic and its large surface area consumes water. Conversely, rGO increases the workability of composites owing to its almost hydrophobic nature and the use of superplasticiser in rGO-water solution.
3) Both GO, and rGO increases the rate of heat of hydration during the early age hydration compared to the control mix. The active participation of GO functional groups accelerated cement hydration which reduced the final setting time about an hour compared to the control mix. The final setting time in the rGO composite increased by an hour. However, the magnitude of the rate of heat peak corresponds to $C_2S$, and in particular, $C_3A$ phase hydration increased considerably compared to the control mix. Corresponding to the calorimetric study, the TGA and XRD results suggest that the GO composite have a higher content of $Ca(OH)_2$ and C-S-H compared to the rGO composite followed by the control mix.
4) The morphological and microstructure observation by SEM-EDX suggested that micropores in the GO composite smaller than ~10 μm were commonly filled with amorphous C-S-H gel and a combination of crystalline hydrated products such as $Ca(OH)_2$ (portlandite). GO's high dispersibility in water and small plane size (1.2±0.8 μm) encourage the pore filling performance. Micropores in the rGO composites were filled randomly, and common hydration products were mostly ettringite with partial portlandite and other hydration products. rGO's low dispersibility in water, agglomeration and high plane size (17.5±9.2 μm) limits the small micropore filling performance. Nevertheless, the BET and BJH calculation from the DVS test show that the GO and rGO composites have slightly high C-S-H gel pore (< 2 nm) volume compared to the control mix.
5) The mechanical properties of the GO and rGO composites were improved compared to the control samples. The GO composites have more flexural strengths compared to the rGO composites, while rGO composites have more compressive strength compared to the GO composites. Mechanical properties show increasing trend with the increasing proportions of rGO in the composite. Whereas, optimum performance in the GO composites resulted in the 0.04% GO composite.
6) Mechanical properties improved in GO composites due to GO's high dispersibility in water together with high content functional groups participation in chemical bonding with cement

hydration products which effectively dense and bridged the composite matrix at a nano-micro level. The mechanical properties improved in rGO composites due to rGO's high physical strength and remaining low content functional groups which formed bonding with cement hydration products.

7) The transport properties of both the GO and rGO composites show promising improvement compared to the control samples. The electrical resistivity slightly increased in GO and rGO composites compared to the control samples. Whereas, the water sorptivity coefficient was considerably reduced in the GO composites compared to the rGO composites followed by the control samples.

**Acknowledgements**

The authors are grateful for support from Professor Panesar's NSERC, Canada Discovery Grant and her Erwin Edward Hart Early Career Award.

**References**

[1] S. Stankovich, D.A. Dikin, G.H.B. Dommett, K.M. Kohlhaas, E.J. Zimney, E.A. Stach, R.D. Piner, S.T. Nguyen, R.S. Ruoff, Graphene-based composite materials, Nature. 442 (2006) 282–286. doi:10.1038/nature04969.

[2] J. Yang, M. Wu, F. Chen, Z. Fei, M. Zhong, Preparation , characterization , and supercritical carbon dioxide foaming of polystyrene / graphene oxide composites, J. Supercrit. Fluids. 56 (2011) 201–207. doi:10.1016/j.supflu.2010.12.014.

[3] S. Lv, Y. Ma, C. Qiu, T. Sun, J. Liu, Q. Zhou, Effect of graphene oxide nanosheets of microstructure and mechanical properties of cement composites, Constr. Build. Mater. 49 (2013) 121–127. doi:10.1016/j.conbuildmat.2013.08.022.

[4] H. Chu, J. Jiang, W. Sun, M. Zhang, Effects of graphene sulfonate nanosheets on mechanical and thermal properties of sacrificial concrete during high temperature exposure, Cem. Concr. Compos. 82 (2017) 252–264. doi:10.1016/j.cemconcomp.2017.06.007.

[5] M. Saafi, L. Tang, J. Fung, M. Rahman, J. Liggat, Enhanced properties of graphene/fly ash geopolymeric composite cement, Cem. Concr. Res. 67 (2015) 292–299. doi:10.1016/j.cemconres.2014.08.011.

[6] M.M. Mokhtar, S.A. Abo-El-Enein, M.Y. Hassaan, M.S. Morsy, M.H. Khalil, Mechanical performance, pore structure and micro-structural characteristics of graphene oxide nano platelets reinforced cement, Constr. Build. Mater. 138 (2017) 333–339. doi:10.1016/j.conbuildmat.2017.02.021.

[7] H. Yang, M. Monasterio, H. Cui, N. Han, Experimental study of the effects of graphene oxide on microstructure and properties of cement paste composite, Compos. Part A Appl. Sci. Manuf. 102 (2017) 263–272. doi:10.1016/j.compositesa.2017.07.022.

[8] M. Murugan, M. Santhanam, S. Sen Gupta, T. Pradeep, S.P. Shah, Influence of 2D rGO nanosheets on the properties of OPC paste, Cem. Concr. Compos. 70 (2016) 48–59. doi:10.1016/j.cemconcomp.2016.03.005.

[9] A. Gholampour, M. Valizadeh Kiamahalleh, D.N.H. Tran, T. Ozbakkaloglu, D. Losic, From Graphene Oxide to Reduced Graphene Oxide: Impact on the Physiochemical and Mechanical Properties of Graphene–Cement Composites, ACS Appl. Mater. Interfaces. (2017) acsami.7b16736. doi:10.1021/acsami.7b16736.

[10] X. Li, A.H. Korayem, C. Li, Y. Liu, H. He, J.G. Sanjayan, W.H. Duan, Incorporation of graphene oxide and silica fume into cement paste: A study of dispersion and compressive strength, Constr. Build. Mater. 123 (2016) 327–335. doi:10.1016/j.conbuildmat.2016.07.022.

[11] O.C. Compton, S.T. Nguyen, Graphene Oxide, Highly Reduced Graphene Oxide, and Graphene: Versatile Building Blocks for Carbon-Based Materials, Small. 6 (2010) 711–723. doi:10.1002/smll.200901934.

[12] T.N. Lambert, C.A. Chavez, B. Hernandez-Sanchez, P. Lu, N.S. Bell, A. Ambrosini, T. Friedman, T.J. Boyle, D.R. Wheeler, D.L. Huber, Synthesis and Characterization of Titania−Graphene Nanocomposites, J. Phys. Chem. C. 113 (2009) 19812–19823. doi:10.1021/jp905456f.

[13] H. Yang, H. Cui, W. Tang, Z. Li, N. Han, F. Xing, A critical review on research progress of graphene/cement based composites, Compos. Part A Appl. Sci. Manuf. 102 (2017) 273–296. doi:10.1016/j.compositesa.2017.07.019.

[14] S. Park, J. An, I. Jung, R.D. Piner, S.J. An, X. Li, A. Velamakanni, R.S. Ruoff, Colloidal suspensions of highly reduced graphene oxide in a wide variety of organic solvents, Nano Lett. 9 (2009) 1593–1597. doi:10.1021/nl803798y.

[15] S. Dixit, A. Mahata, D.R. Mahapatra, S. V. Kailas, K. Chattopadhyay, Multi-layer graphene reinforced aluminum – Manufacturing of high strength composite by friction stir alloying, Compos. Part B Eng. 136 (2018) 63–71. doi:10.1016/j.compositesb.2017.10.028.

[16] K. Erickson, R. Erni, Z. Lee, N. Alem, W. Gannett, A. Zettl, Determination of the Local Chemical Structure of Graphene Oxide and Reduced Graphene Oxide, Adv. Mater. 22 (2010) 4467–4472. doi:10.1002/adma.201000732.

[17] Z. Pan, L. He, L. Qiu, A.H. Korayem, G. Li, J.W. Zhu, F. Collins, D. Li, W.H. Duan, M.C. Wang, Mechanical properties and microstructure of a graphene oxide–cement composite, Cem. Concr. Compos. 58 (2015) 140–147. doi:10.1016/j.cemconcomp.2015.02.001.

[18] E. Horszczaruk, E. Mijowska, R.J. Kalenczuk, M. Aleksandrzak, S. Mijowska, Nanocomposite of cement/graphene oxide - Impact on hydration kinetics and Young's modulus, Constr. Build. Mater. 78 (2015) 234–242. doi:10.1016/j.conbuildmat.2014.12.009.

[19] K. Gong, Z. Pan, A.H. Korayem, L. Qiu, D. Li, F. Collins, C.M. Wang, W.H. Duan, Reinforcing Effects of Graphene Oxide on Portland Cement Paste, J. Mater. Civ. Eng. 27 (2015) A4014010. doi:10.1061/(ASCE)MT.1943-5533.0001125.

[20] H. Cui, X. Yan, L. Tang, F. Xing, Possible pitfall in sample preparation for SEM analysis - A discussion of the paper “Fabrication of polycarboxylate/graphene oxide nanosheet composites by copolymerization for reinforcing and toughening cement composites” by Lv et al., Cem. Concr. Compos. 77 (2017) 81–85. doi:10.1016/j.cemconcomp.2016.12.007.

[21] W. Li, X. Li, S.J. Chen, Y.M. Liu, W.H. Duan, S.P. Shah, Effects of graphene oxide on early-age hydration and electrical resistivity of Portland cement paste, Constr. Build. Mater. 136 (2017) 506–514. doi:10.1016/j.conbuildmat.2017.01.066.

[22] A. Mohammed, J.G. Sanjayan, W.H. Duan, A. Nazari, Incorporating graphene oxide in cement composites: A study of transport properties, Constr. Build. Mater. 84 (2015) 341–347. doi:10.1016/j.conbuildmat.2015.01.083.

[23] C. Qiu, Q. Zhou, S. Lv, Y. Ma, Regulation of GO on cement hydration crystals and its toughening effect, Mag. Concr. Res. 65 (2013) 1246–1254. doi:10.1680/macr.13.00190.

[24] G. Bastos, F. Patiño-Barbeito, F. Patiño-Cambeiro, J. Armesto, Admixtures in Cement-Matrix Composites for Mechanical Reinforcement, Sustainability, and Smart Features, Materials (Basel). 9 (2016) 972. doi:10.3390/ma9120972.

[25] S. Chuah, Z. Pan, J.G. Sanjayan, C.M. Wang, W.H. Duan, Nano reinforced cement and concrete composites and new perspective from graphene oxide, Constr. Build. Mater. 73 (2014) 113–124. doi:10.1016/j.conbuildmat.2014.09.040.

[26] W. Lv, Z. Li, Y. Deng, Q.-H. Yang, F. Kang, Graphene-based materials for electrochemical energy storage devices: Opportunities and challenges, Energy Storage Mater. 2 (2016) 107–138. doi:10.1016/j.ensm.2015.10.002.

[27] Y. Zhu, S. Murali, W. Cai, X. Li, J.W. Suk, J.R. Potts, R.S. Ruoff, Graphene and Graphene Oxide: Synthesis, Properties, and Applications, Adv. Mater. 22 (2010) 3906–3924. doi:10.1002/adma.201001068.

[28] L. Zhao, X. Guo, C. Ge, Q. Li, L. Guo, X. Shu, J. Liu, Mechanical behavior and toughening mechanism of polycarboxylate superplasticizer modified graphene oxide reinforced cement composites, Compos. Part B Eng. 113 (2017) 308–316. doi:10.1016/j.compositesb.2017.01.056.

[29] T.S. Qureshi, D.K. Panesar, S. Boopathi, A. Chen, P.C. Wood, Nano-cement composite with graphene oxide produced from epigenetic graphite deposit, Compos. Part B. (2018). doi:DOI: 10.1016/j.compositesb.2018.09.095.

[30] S. Sun, S. Ding, B. Han, S. Dong, X. Yu, D. Zhou, J. Ou, Multi-layer graphene-engineered cementitious composites with multifunctionality/intelligence, Compos. Part B Eng. 129 (2017) 221–232. doi:10.1016/j.compositesb.2017.07.063.

[31] S.K. Mishra, S.N. Tripathi, V. Choudhary, B.D. Gupta, SPR based fibre optic ammonia gas sensor utilizing nanocomposite film of PMMA/reduced graphene oxide prepared by in situ polymerization, Sensors Actuators, B Chem. 199 (2014) 190–200. doi:10.1016/j.snb.2014.03.109.

[32] C. Chen, M. Long, M. Xia, C. Zhang, W. Cai, Reduction of graphene oxide by an in-situ photoelectrochemical method in a dye-sensitized solar cell assembly., Nanoscale Res. Lett. 7 (2012) 101. doi:10.1186/1556-276X-7-101.

[33] S. Eigler, C. Dotzer, A. Hirsch, Visualization of defect densities in reduced graphene oxide, Carbon N. Y. 50 (2012) 3666–3673. doi:10.1016/J.CARBON.2012.03.039.

[34] BS EN:196-1, Methods of testing cement. Determination of strength, Br. Stand. Inst. (2005).

[35] F. Collins, J. Lambert, W.H. Duan, The influences of admixtures on the dispersion, workability, and strength of carbon nanotube-OPC paste mixtures, Cem. Concr. Compos. 34 (2012) 201–207. doi:10.1016/j.cemconcomp.2011.09.013.

[36] ASTM Standard C1437-07, Standard Test Method for Flow of Hydraulic Cement Mortar, 2007. doi:10.1520/C1437-07.

[37] D.K. Panesar, J. Francis, Influence of limestone and slag on the pore structure of cement paste based on mercury intrusion porosimetry and water vapour sorption measurements, Constr. Build. Mater. 52 (2014) 52–58. doi:10.1016/J.CONBUILDMAT.2013.11.022.

[38] ASTM C109 / C109M-16a, Standard Test Method for Compressive Strength of Hydraulic Cement Mortars (Using 2-in. or [50-mm] Cube Specimens), 2016. doi:10.1520/C0109_C0109M-16A.

[39] ASTM C348-14, Standard Test Method for Flexural Strength of Hydraulic-Cement Mortars, 2014. doi:10.1520/C0348-14.

[40] H. Layssi, P. Ghods, A.R. Alizadeh, M. Salehi, Electrical resistivity of concrete, Concr. Int. 37 (2015) 41–46.

[41] O. Sengul, Use of electrical resistivity as an indicator for durability, Constr. Build. Mater. 73 (2014) 434–441. doi:10.1016/j.conbuildmat.2014.09.077.

[42] C. Hall, T.K.-M. Tse, Water movement in porous building materials—VII. The sorptivity of mortars, Build. Environ. 21 (1986) 113–118. doi:10.1016/0360-1323(86)90017-X.

[43] T.S. Qureshi, A. Al-Tabbaa, Self-healing of drying shrinkage cracks in cement-based materials incorporating reactive MgO, Smart Mater. Struct. 25 (2016) 084004. doi:10.1088/0964-1726/25/8/084004.

[44] R. Roychand, S. De Silva, D. Law, S. Setunge, High volume fly ash cement composite modified with nano silica, hydrated lime and set accelerator, Mater. Struct. 49 (2016) 1997–2008. doi:10.1617/s11527-015-0629-z.

[45] F. Babak, H. Abolfazl, R. Alimorad, G. Parviz, Preparation and mechanical properties of graphene oxide: cement nanocomposites., ScientificWorldJournal. 2014 (2014) 276323. doi:10.1155/2014/276323.

[46] Z.S. Chen, X. Zhou, X. Wang, P. Guo, Mechanical behavior of multilayer GO carbon-fiber cement composites, Constr. Build. Mater. 159 (2018) 205–212. doi:10.1016/j.conbuildmat.2017.10.094.

[47] V. Baroghel-Bouny, Water vapour sorption experiments on hardened cementitious materials: Part I: Essential tool for analysis of hygral behaviour and its relation to pore structure, Cem. Concr. Res. 37 (2007) 414–437. doi:10.1016/J.CEMCONRES.2006.11.019.

[48] D. Zhao, J. Chen, Q. Gao, H.Y. Ge, Graphene Oxide/Cement Composites for Electromagnetic Interference Shielding, Mater. Sci. Forum. 809-810 (2014) 485–489. doi:10.4028/www.scientific.net/MSF.809-810.485.